JOURNAL OF MATERIALS SCIENCE **34** (1999) 2561–2564

Study of overgrowth heterostructure InSb/GaAs by scanning electron acoustic microscopy

SHUWEI LI*, ERICH KUBALEK
Materials for Electrical Engineering, Gerhard-Mercator-University Duisburg, 47048 Duisburg, Germany

YIXIN JIN
Changchun Institute of Physics, Chinese Academy of Sciences, 130021 Changchun, People's Republic of China

FUMING JIANG, QINGRUI YIN
Shanghai Institute of Ceramics, Chinese Academy of Sciences, 200050 Shanghai, People's Republic of China

An overgrowth InSb epilayer on GaAs substrate with large lattice-mismatch was grown by metalorganic chemical vapor deposition (MOCVD), and the heterogeneous crystalline state was observed by scanning electron acoustic microscopy (SEAM). The middle stage of relaxation of the large mismatch InSb/GaAs epilayer is observed by SEAM images of crystalline state of the buried subsurfaces. A macroscopical heterogeneous distribution is formed by large compression stress fields. It was a very important result to observe and study semiconductor epitaxial heterostructures by SEAM uniquely imaging mechanism.

1. Introduction

Heteroepitaxial structures are widely used in optical, acoustic, electronic and magnetic device and have become increasingly important in electronic and optoelectronic device applications [1, 2]. The process of plastic relaxation of the large lattice mismatch, which leads to a degradation of the device performance [3], and crystalline state of the buried subsurface must be well understood in order to decrease the plastic relaxation by controlling the key growth parameters.

Recently, the growth of the heteroepitaxial InSb/GaAs has received increasing interest [4, 5]. First, the material with the large lattice mismatch (14.5%) is easy to observe and study the relaxation of the large lattice-mismatch. Second, as an infrared detector the heteroepitaxial InSb/GaAs is a potential heteroepitaxial structure. Third, it can be used for high speed electronic and magnetic Hall devices. Fourth, semi-insulating GaAs is a desirable substrate to analyze electrical properties of InSb epilayer. Fifth, GaAs material allows integration of infrared detection and signal processing devices on the same substrate.

Scanning electron acoustic microscopy (SEAM) was developed in 1980 [6] and has been mainly used in the last few years in the characterization of thermal, elastic and pyroelectric properties on a microscale resolution [7]. It has been successively reported as a non-destructive experimental tool for study of polarization distribution, phase transition, subgrain boundary and domain structure in polar materials and non-destructive observation of internal phenomena in many other materials and devices [8]. Balk, Kultscher, and Kaufmann *et al*. [9, 10] studied signal generation and contrast mechanism of Silicon and III-V semiconductor compounds. Recently, SEAM was reported to study crystalline quality and defect growth of semiconductor epilayers [11, 12]. In this paper, the middle stage of mismatch relaxation and heterogeneous crystalline state of large mismatch InSb/GaAs epilayer are observed and studied by SEAM.

2. Epitaxial growth

The InSb epilayer was grown on a GaAs substrate by MOCVD using a conventional atmospheric pressure horizontal reactor. The sources of In and Sb were trimethylindium (TMIn) and trimethylantimony (TMSb), respectively. TMIn and TMSb were respectively held at 17 and $-10\,^{\circ}$C by using temperature baths and carried by Pd-diffused hydrogen into reactor. The substrate was semi-insulating GaAs which was oriented 2–3° off (001) towards ⟨110⟩. III/V ratio was 0.5, the total gas flow into the reactor was 4 l/min, the growth temperature was 520 °C the growth time was 180 min, and the epitaxial thickness was 7 μm.

3. Experiment of SEAM

Figs 1–3 show scanning electron microscopy (SEM) images of the epitaxial surface and *in-situ* SEAM

* Author to whom all correspondence should be addressed.

images of buried subsurfaces in three different positions of the InSb/GaAs epilayer. The set-up of the electron acoustic experiment is constructed using conventional scanning electron microscopy to which several newly designed parts, a flexible plug-in beam blanking system, an opto-electronic coupler and a spring loaded and metal shielded PZT (piezoelectric ceramic transducer) electron acoustic signal detector, are attached. A chopping system consisting of a pair of condenser plates and a flexible plug-in beam blanking electronics to create a periodically modulated beam is used. The chopping electron beams generate both acoustic and thermal waves in samples clamped on a PZT, which is often explained by the conversion of an electron-beam-induced heat distribution by means of the thermal expansion coefficient [6, 13]. The thermal wave component generated in the material is highly attenuated, in practice, and the information recorded from the transducer attached to a thermally thick sample depends on the received acoustic wave component. The electron beam characteristics were chopping frequency from 30 to 500 kHz, duty ratio of 50%, acceleration voltage of 20–30 kV, and maximum beam current of 4×10 μA.

The dislocation reacts strongly to the acoustic wave, which is especially sensitive to variations in elastic properties. So, accumulation of dislocations easy to be detected, and crystalline state of the buried subsurfaces may be observed by SEAM. The crystal thickness equation of the buried subsurface is $d = (2k/f\rho c)^{1/2}$ [6] (f the acoustic frequency, ρ the density, c the specific heat, and k the thermal conductivity at SEAM-working-temperature). The (001) growth direction in zincblend structure semiconductors does not induce a piezoelectric field [14, 10]. So, the piezoelectric coupling was not considered. Comparisons are made between standard SEM image and SEAM images taken at different chopping frequencies. Therefore, a surface image and in-situ buried subsurface images with different depths can be observed to study the epitaxial crystalline state.

4. Discuss of SEAM experiment

SEAM images may provide information of epitaxial crystalline state, and SEM images may provide the surface morphology *in situ*. Comparison of Fig. 1a–d show two differently imaging techniques. Chopping frequencies of SEAM images (d), (c) and (b) were 140, 149 and 170 kHz, and the corresponding subsurface depths were -4.6, -4.4, and -3.9 μm, respectively.

In a large lattice-mismatch heteroepitaxial InSb/GaAs, the lattice parameter of the first atomic layers deposited on a substrate are strained to match the substrate lattice parameter. The epilayer thickness increases with increasing strain energy and stress field to h_c where the first misfit-relieving dislocation produces [15]. At the critical thickness, the accumulated strain energy imposes the equilibrium situation which corresponds to a 3D configuration of the epitaxial film [16]. Since

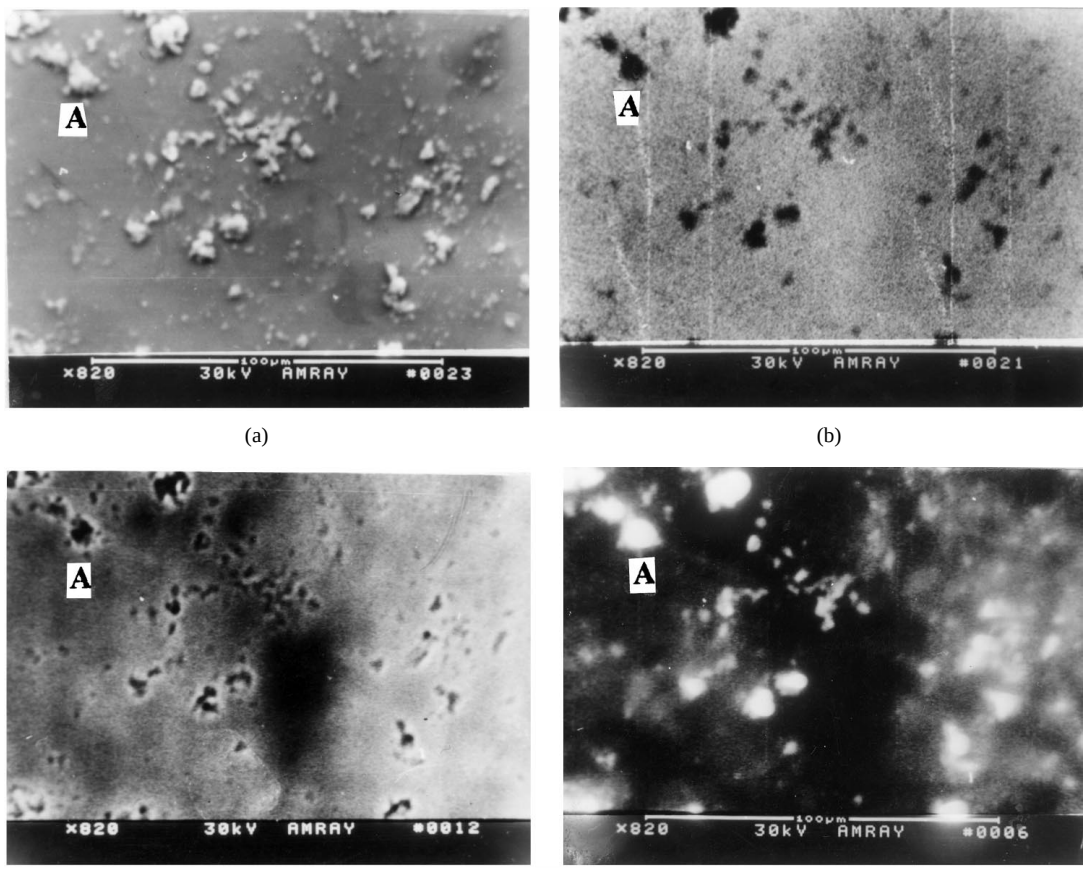

Figure 1 (a) The scanning electron microscopy image, (b) the scanning electron acoustic microscopy image $f = 170$ kHz, (c) the scanning electron acoustic microscopy image $f = 149$ kHz, and (d) the scanning electron acoustic microscopy image $f = 140$ kHz. In Fig. 1d SEAM image with the depth is $d = -4.6\,\mu$m, in Fig. 1c SEAM image with the depth is $d = -4.4\,\mu$m, and in Fig. 1b SEAM image with the depth is $d = -3.9\,\mu$m.

a critical thickness h_c decreases with the increasing lattice mismatch of heteroepitaxial system, and a heteroepitaxial InSb/GaAs has a very thin critical thickness. Then, two-dimensional growth fail very quickly and two-dimensional plus three-dimensional Stranski-Krastanov mode is occurred. When growth parameters are suitable, the large mismatch stress may be released by a homogeneous way of regular three-dimensioned islands and a sessile 90° dislocation network [17]. When growth rate is very large to an overgrowth, atomic diffusion time is very small, diffusion length is very short, and the surface diffusion process is insufficient. After many hundreds of monolayers have been deposited, the epitaxial surface gets rough, and the large compression stress fields begin to form a macroscopical heterogeneous distribution. For fast relaxation the large compression stress fields squeeze a certain region to tilt deposited crystalline plane for reduction of the deposited space to fit partially the lattice-match to substrate. Because contrasts of signal generation are sensitive to crystalline directions [18], two different crystalline directions product the bright and dark areas shown in Fig. 1c and d. The boundaries between the bright and dark areas accumulate multitudinous edge-type dislocations due to the SEAM capability to image them. In Fig. 1d and c the dislocation density of the boundaries is in the order of at least 10^8 cm^{-2}. In this fast relaxation stage, the layer is thick enough to produce multiplication of heterogeneous edge-type dislocations and 3D islands. In Fig. 1d SEAM image with the depth $d = -4.6\,\mu$m there was a black region, in Fig. 1c SEAM image with the depth $d = -4.4\,\mu$m this black region became very small, and in Fig. 1b SEAM image with the depth $d = -3.9\,\mu$m this black region disappears. It illustrates that this isolated black region was a big twin surrounded by multiplication of edge-type dislocations, and the twin has a deposited disorientation crystalline planes. In other words, the large compression stress fields affected epitaxial growth to produce a tilt deposited crystalline plane in a certain region to adjust the deposited space to release huge lattice mismatch, and lattice-match GaAs substrate, and form a big twin which is observed by *in situ* three SEAM images. Finally, when relaxation is achieved, the level of relaxation is the saturation state [19]. The structural features of Fig. 1b SEAM image is also visible on the Fig. 1a *in situ* SEM image, which shows that this is a saturation state stage.

In Fig. 2c SEAM image with a chopping frequency $f = 109$ kHz and the depth of the buried subsurface $d = -5.6\ \mu$m, the boundary between the black and white regions are regarded as heterogeneous edge-type dislocations, too. In Fig. 2b the other SEAM image with a frequency $f = 180.7$ kHz and the depth $d = -3.8\,\mu$m, the size and shape of the boundary are not changed, which illustrates that 100% relaxation is not achieved, the saturation state do not occurs. A reversed contrast of Fig. 2b is observed in comparison to Fig. 2c due to change of phase ϕ of the electron acoustic waves. In Fig. 3 chopping frequencies of SEAM images (c) and (b) are 132 and 150 kHz, and the corresponding subsurface crystal depths are -4.8 and $-4.4\,\mu$m, respectively.

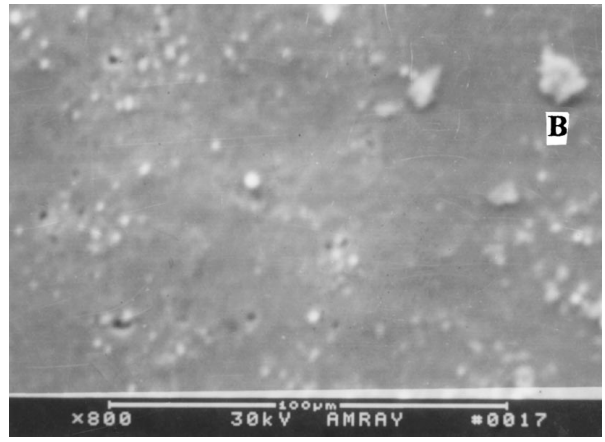

(a)

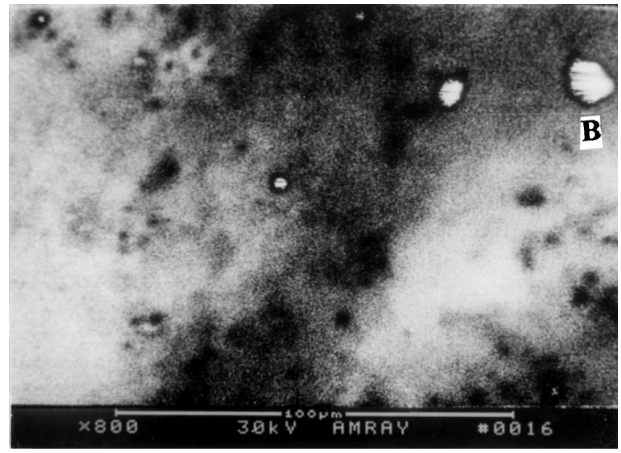

(b)

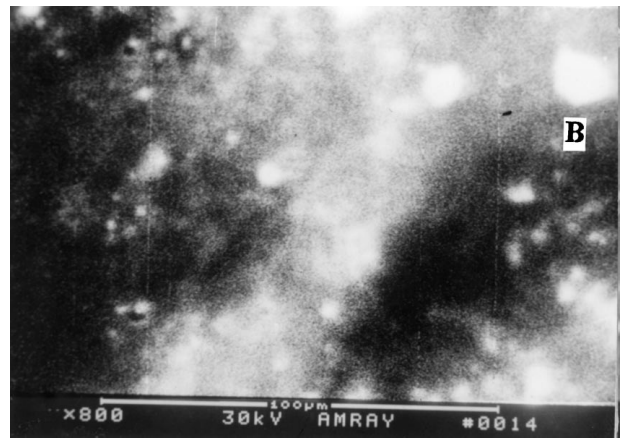

(c)

Figure 2 (a) The scanning electron microscopy image, (b) the scanning electron acoustic microscopy image $f = 180.7$ kHz, and (c) the scanning electron acoustic microscopy image $f = 109$ kHz. In Fig. 2c SEAM image with the crystal depth of the buried subsurface is $d = -5.6\,\mu$m, and in Fig. 1b SEAM image with the depth $d = -3.8\,\mu$m.

Structural features of two SEAM subsurface images are also visible on the *in-situ* SEM surface image, which means that the images contain information of the surface topography. So, it shows that at the subsurface of the depth $-4.8\,\mu$m 100% relaxation has been achieved, and the saturation state has occurred.

From SEAM images of the three positions 100% large mismatch relaxation is not simultaneously achieved, and the saturation state happened in different

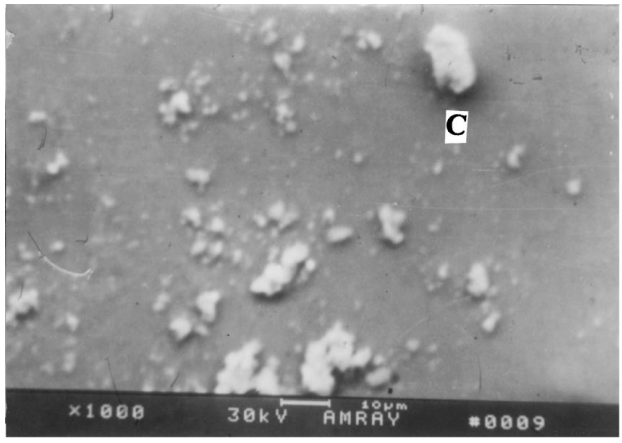

(a)

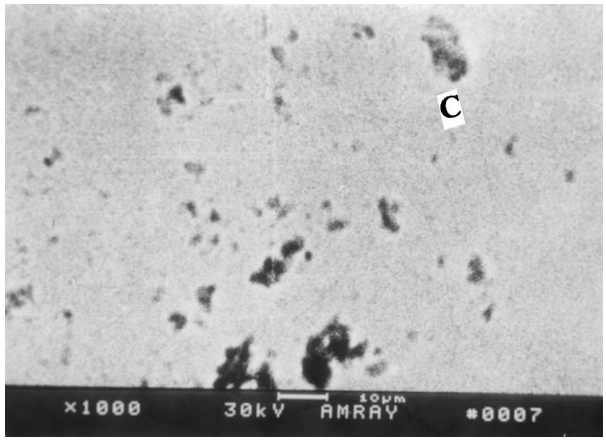

(b)

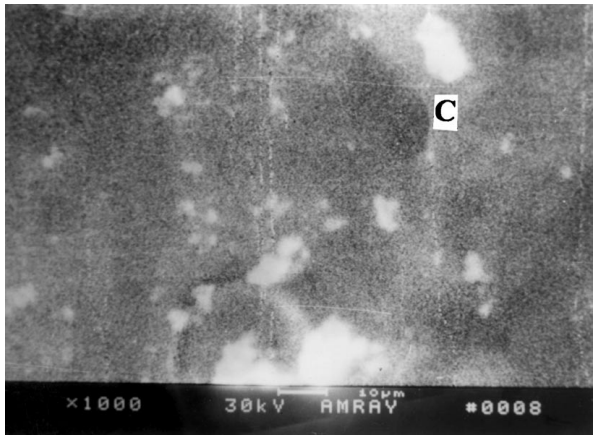

(c)

Figure 3 (a) The scanning electron microscopy image, (b) the scanning electron acoustic microscopy image $f = 150$ kHz, and (c) the scanning electron acoustic microscopy image $f = 132$ kHz. In Fig. 2c SEAM image with the crystal depth of the buried subsurface is $d = -4.8\,\mu$m, and in Fig. 1b SEAM image with the depth is $d = -4.4\,\mu$m.

subsurfaces, which shows the crystalline state of a macroscopical heterogeneous distribution.

In Figs 1–3 images, a lot of irregular three-dimensional islands may be observed. In the relaxation stage from Fig. 1d to c the 3D island A becomes small, and in the saturation state stage from Fig. 1b to a the 3D island A is not changed. Similarly, in the relaxation stage from Fig. 2c to b 3D island B becomes small, and in saturation state stage from Fig. 3c to a the 3D island C is not changed. It shows the 3D islands produced by large lattice mismatch gradually become small with the decreasing relaxation, and their shapes nearly are not changes in the saturation state stage.

5. Conclusion

It is very important field to study crystalline properties in large lattice-mismatch heteroepitaxial systems. The crystalline information of the buried subsurface is especially important to be understood because the buried subsurface irregularity affects the device performance. Due to the lack of suitable characterization techniques, structure of epitaxial subsurfaces and interface has been a subject of much speculation. Scanning electron acoustic microscopy as a non-destructive experimental tool to study the buried subsurfaces and interface of semiconductor materials is quite significant. In the large mismatch system of InSb/GaAs epilayer the crystalline state of a macroscopical heterogeneous distribution were studied successfully, and the epitaxial growth stage of the relaxation and saturation state are observed by SEAM images of the buried subsurfaces.

Acknowledgement

Dr. S. Li is receiving financial support from Alexander von Humboldt Foundation for a research fellow.

References

1. J. Y. TSAO and B. W. DODSON, *Appl. Phys. Lett.* **53** (1988) 848.
2. J. ZHOU, *Thin Solid Films* **235** (1993) 6.
3. N. GRANDJEAN and J. MASSIES, *J. Crystal Growth* **134** (1993) 51.
4. M. BEHET, B. STOLL and K. HEIME, *ibid.* **135** (1994) 434.
5. R. M. BIEFELD and G. A. HETNER, *ibid.* **109** (1991) 272.
6. G. S. CARGILL III, *Nature* **286** (1980) 691.
7. M. URCHULUTEGUI and J. PIQUERAS, *J. Appl. Phys.* **67** (1990) 1.
8. P. FERNANDEZ, J. LLOPIS and J. PIQUERAS, *Materials Chemistry Physics* **24** (1989) 215.
9. L. J. BALK and N. KULTSCHER, *Inst. Phys. Conf. Ser.* **87**, Sect. II (1987) 675.
10. K. KAUFMANN, K. ORSECH, M. DOMNIK and L. J. BALK, *J. Phys. D: Appl. Phys.* **27** (1994) 2401.
11. SHUWEI LI, Y IXIN JIN, BAOLIN ZHANG, YONGQIANG NING, TIANMING ZHOU, HONG JIANG and GUANG YUAN, *Solid State Communications* **97** (1996) 975.
12. SHUWEI LI, FUMING JIANG, QINGRUI YIN and YIXIN JIN, *ibid.* **99** (1996) 853.
13. M. URCHULUTEGUI, J. PIQUERAS and J. LLOPIS *J. Appl. Phys.* **65** (1989) 2677.
14. D. L. SMITH, *Solid State Communications* **57** (1986) 919.
15. M. LENTZEN, D. GERTHSEN, A. FORSTER and K. URBEN, *Appl. Phys. Lett.* **60** (1992) 74.
16. N. GRANDJEAN and J. MASSIES, *J. Crystal Growth* **134** (1993) 51.
17. SHUWEI LI, YONGQIANG NING, TIANMING ZHOU, YIXIN JIN and YUAN TIAN, *Thin Solid Film* **298** (1997) 245.
18. L. J. BALK, in "Analysis of Miroelectronic Materials and Devices," edited by M. Grasserbauer and H. W. Werner (J. Wiley and Sons, Chichester-New York, 1991) p. 741.
19. D. GONZALEZ, D. ARAUJO, G. ARAGON and R. GARCIA, *Appl. Phys. Lett.* **71** (1997) 2475.

Received 24 July
and accepted 23 December 1998